

Univariate Prediction of Hammett Parameters and Select Relative Reaction Rates Using Loewdin Atomic Charges

Gautam D. Stroschio^{a*}, and Nir Goldman^{a, b}

^aLawrence Livermore National Laboratory, Livermore, California 94550, United States.

^bDepartment of Chemical Engineering, University of California, Davis, California 95616, United States.

SUBJECTS: Hammett Parameters, Nitroarenes, Photochemistry, 9-(4-X-phenyl)-9H-fluorene Substrates, C-H Activation, Electronic Structure Calculations, Reaction Rates.

ABSTRACT: Loewdin charges from density functional theory calculations have been used here to obtain general, univariate linear correlations for the prediction of experimental Hammett parameters and relative reaction rates. While previous studies have established that Hirshfeld and CM5 charges perform strongly as univariate predictors, the near-ubiquitous Loewdin charges have not yet been evaluated. To this end, we assess the predictive capability of Loewdin charges for three chemical systems. First, we show that Loewdin charges outperform Hirshfeld and CM5 charges for Hammett parameter prediction. Second, we see Loewdin charges generally perform comparably to Hirshfeld charges for predicting the relative rates of olefin cleavage by photoexcited nitroarenes. The single case of poor correlation, between relative rates and the Loewdin charges on nitrogen sites, is ameliorated when considering the net charge on the NO₂ group. Third, we show that Loewdin, Hirshfeld, and CM5 charges all perform very well for generating correlations for relative reaction rates for C-H activation of 9-(4-X-phenyl)-9H-fluorene substrates by a transition metal catalyst. The equations generated throughout the study enable the prediction of Hammett parameters and relative reaction rates. These tools can accelerate synthetic and experimental studies by enabling the *in silico* prediction of uncharacterized chemical properties.

Introduction

Originally obtained as an empirical descriptor of how para- (σ_p) or meta- (σ_m) substituents correlate with experimental values of benzoic acid ionization constants in water,^{1,2} Hammett parameters have been used to predict electronic substituent effects on reaction rates and

equilibrium constants in effectively every class of organic reaction.^{3,4} By quantifying the inductive and resonance effects from para- and meta-aromatic substituents, σ_p and σ_m have facilitated the generation of innumerable predictive linear correlations between electronic effects of chemical composition and properties. Indeed, the success of Hammett parameters has inspired the development of related variant experimental parameters; these were obtained from additional reference processes and measured properties including ionization of phenols (σ^-),² heterolysis of cumyl chlorides (σ^+),⁵ methylenecyclopropane rearrangements (σ_C),⁶ cyclodimerizations of trifluorostyrenes (σ_{ij}),⁷ and benzyl radical hyperfine coupling constants from electron paramagnetic resonance measurements (σ_a).⁸ In addition to experiment, the predictive power of Hammett parameters has also inspired theoretical and computational research. Several recent computational studies have focused on facilitating the prediction of Hammett parameters for yet unstudied systems.^{9–11}

Amongst these recent computational studies is a density functional theory (DFT) benchmarking investigation from Luchini and Paton.⁹ Through the assessment of many different classes of potential predictors, they have demonstrated that several Class II charge models^{12,13} (models based on partitioning the quantum mechanical charge density) and Class IV charge models (semi-empirical corrections to Class II models) are among the best predictors of Hammett parameters. As a result, the authors propose that linear regression formulas relating the experimental parameters to the computed charges provide a reliable, single variable (univariate) means of computationally predicting σ_p , σ_m , or even select relative rate constants via $\log_{10}(k/k_H)$ (where k_H is the reference rate and k/k_H can be equivalently denoted as k_{rel}).

However, open questions remain regarding the optimal determination of these linear relationships. For example, it was observed that the identity of the Class II or IV charge model largely determined the accuracy of the fit, rather than the level of theory (*e.g.*, the DFT exchange-correlation functional or basis set) in the underlying electronic structure calculation.⁹ Charge models that partition the density using projection of the wave function (*e.g.*, Mulliken charges¹⁴ and the commonly used Natural Population Analysis or NPA charges^{15,16}) were seen to fare worse than those that directly partition the density (*e.g.*, Hirshfeld charges¹⁷ and their Class IV counterpart CM5¹⁸ charges). In addition, the choice of the specific atomic site used in the fit had a significant effect on the quality of the obtained linear regression; for Hammett parameter prediction, the use of carbon atoms located para- or meta- to the substituent group often yielded

worse correlations, in contrast to the use of the hydrogen atom bonded to that carbon.⁹ For many charge models, this lack of predictive consistency with respect to the utilized atomic location was also seen when trying to predict relative rates of olefin cleavage by photoexcited nitroarenes.^{9,19} Further assessment of different, additional charge-based methodologies could potentially result in more accurate, robust predictions. This would be particularly valuable for investigations without access to Hirshfeld and CM5 datasets.

Loewdin atomic charges^{20,21} (developed by Per-Olov Löwdin and usually spelled Löwdin, but here spelled Loewdin to be consistent with the output of many quantum chemistry packages) are a near-ubiquitous charge model that was not among those previously studied.⁹ It is similar to NPA, in that it is a systematic improvement of the Mulliken charge model. It has provided useful insights for a wide variety of chemical systems including the characterization of molecular orbitals and states in multireference wave function method studies of systems as different as chromium(IV) molecular qubit candidates²² and iron-porphyrin carbene reactive intermediates.²³ Given the ubiquity and prevalence of Loewdin charges, their use in the generation of predictive, univariate linear correlations would further enable the characterization of chemical reactivity.

Indeed, here we use Loewdin charges to generate predictive, univariate linear correlations for three test cases: (1) experimental σ_p and σ_m parameters, (2) $\log_{10}(k_{rel})$ values for olefin cleavage by photoexcited nitroarenes, and (3) $\log_{10}(k_{rel})$ values for C-H activation^{24,25} of 9-(4-X-phenyl)-9H-fluorene substrates by a transition metal catalyst. To assess the quality of these linear correlations, comparisons to correlations using Hirshfeld, CM5, and NPA charges are made. Both previously published and newly obtained (when needed) correlations are used for the comparisons to the Loewdin results. For a subset of our results, Loewdin atomic charges are superior to all previously assessed charge models when judged by the Pearson's R^2 value and the mean absolute error (MAE) of the obtained linear fit. In other cases, results from Loewdin charges are comparable to those from Hirshfeld and CM5 charges. The third examined test case is notable due to the large size of the organic substrate and the complexity of the studied chemical systems (*vide infra*). Finally, we present equations from all three parts of this study that will enable the accurate prediction of new values of σ_p , σ_m , and $\log_{10}(k_{rel})$ values.

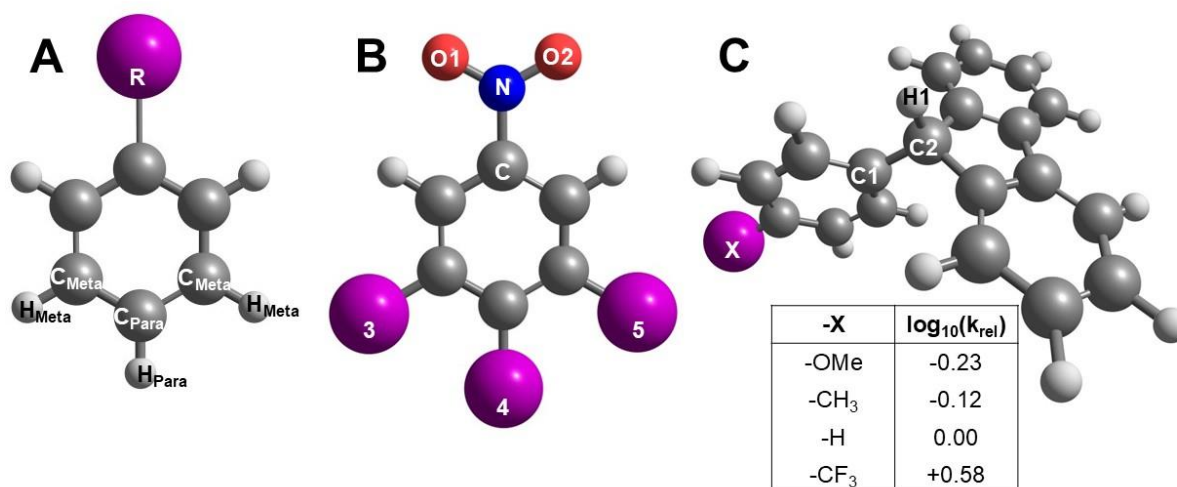


Figure 1. The three studied systems are shown above with carbons in gray, hydrogens in white, nitrogens in blue, oxygens in red, and generic substituent groups in purple. The substituted benzene molecule in **A** has the meta and para positions identified; -R represents one of the 89 substituents studied here and in Ref. 9. The nitroarene in **B** has the atoms for which Loewdin and Hirshfeld atomic charges were tabulated (C, N, O1, and O2). Also shown are the numberings used by Ruffoni *et al.* in Ref. 19 to identify the locations of the substituent functional groups relative to the NO₂ functional group. The generalized 9-(4-X-phenyl)-9H-fluorene substrate in **C** (X = OMe, CH₃, H, or CF₃) includes identification of the atoms for which computed charges were tabulated: C1, C2, and H1. The inset includes $\log_{10}(k_{rel})$ values for C-H activation, as measured by Goetz and Anderson in Refs. 24 and 25.

Computational Methods

To provide the closest comparison to the previous examinations correlating computed atomic charge to experimental Hammett parameters, this study examined the DFT optimized structures made publicly available by Luchini and Paton.^{9,26} This database consists of 89 substituted benzene molecules with experimentally known σ_p and σ_m parameters. These 178 experimental values were also used by Ertl in the development of a free web tool for Hammett parameter prediction¹¹ and by Monteiro-de-Castro *et al.* in their machine learning study of multivariate Hammett parameter prediction.¹⁰ The geometric structures provided by Luchini and Paton in their database had been previously optimized using the B3LYP^{27,28} DFT functional, the

def2-TZVP^{29,30} basis set, Grimme *et al.*'s D3 dispersion energy correction using Becke-Johnson damping^{31,32} [D3(BJ)], and the SMD implicit solvation model³³ for chloroform.

In the sections of the present study examining Hammett parameters and relative rates of olefin cleavage by photoexcited nitroarenes, atomic charges were obtained from single point DFT calculations using the same level of theory used in the published geometry optimizations described above (example input provided in the SI). These new calculations were performed using ORCA³⁴⁻³⁸ version 5.0.4 using a self-consistent field (SCF) energy threshold of 10^{-8} Hartree and the restricted Kohn-Sham (RKS) formalism. The RIJCOSX approximation³⁹ was used in these calculations. Table S1 and S2 in the SI tabulates the electronic energies from these single point calculations. For just one calculation corresponding to structure 7_1 in Table S1, the def2-ECP effective core potential⁴⁰ was applied to a heavier element (iodine), as is the default in ORCA 5.0.4. For the Hammett parameter section, text files containing the tabulated Loewdin atomic charges have been provided among the supplementary materials. For the nitroarene section, Loewdin and newly calculated Hirshfeld charges are tabulated in the SI.

Unlike previous work, only the lowest energy conformer for a given substituted benzene molecule was used to obtain linear correlations between experimental values and calculated atomic charges. Also, only one structure was used when multiple energetically degenerate lowest energy conformers were available. The identities of the used conformers are also tabulated in Table S1 and S2 in the SI using the nomenclature of the Luchini and Paton. We have not performed Boltzmann averaging of atomic charge values from multiple conformers for the sake of computational efficiency, and due to the likely small effect from energetically similar structures. This assumption was indeed borne out to be true by reproduction of the previously observed trends⁹ related to the Hirshfeld nitroarene R^2 results despite any methodological differences in our approach.

The four 9-(4-X-phenyl)-9*H*-fluorene substrates were optimized here using the M06-L⁴¹ DFT functional, the def2-TZVP basis set, and the SMD model for dimethylsulfoxide. These optimizations were performed in Gaussian 16, Rev. A.03,⁴² and verified to be stationary points using the calculations of vibrational frequencies. The closed-shell singlet state was calculated using the RKS formalism and the triplet state was calculated using the unrestricted Kohn-Sham formalism (UKS). For the optimized closed-shell singlet structures, ORCA 5.0.4 was then used for DFT single point calculations using replacing M06-L with B3LYP and keeping all other aspects

of the calculation the same; this same methodology was used for the optimized $S = 1$ structures, except we used the UKS formalism and $S = 1$ for the spin multiplicity. The energetics and charge values from all these DFT calculations are tabulated in the SI.

Results and Discussion

In our Hammett parameter study, atomic charges were tabulated for the ring carbons that are para and meta to the unique substituent functional group. These are visually identified in Figure 1A (Figure S1 also includes labels relevant to the uploaded text files tabulating the Loewdin atomic charges). Atomic charges were also tabulated for the hydrogens bonded to those ring carbons that are para and meta to the unique substituent functional group. Pairs of meta values were averaged into a single carbon or hydrogen meta value. The quality of the correlation of the four obtained atomic charge data sets ($q(C_{\text{Meta}})_{\text{Loewdin}}$, $q(H_{\text{Meta}})_{\text{Loewdin}}$, $q(C_{\text{Para}})_{\text{Loewdin}}$, $q(H_{\text{Para}})_{\text{Loewdin}}$) to the experimental σ_p and σ_m parameters was assessed using linear fits and the resulting Pearson's R^2 value (Figure 2). The insets within Figures 2A-2D contain the newly obtained general, predictive linear relationships that can be used to estimate unknown experimental Hammett parameters for the corresponding substituted benzene.

In all four cases, the linear correlations between experimental Hammett parameters and Loewdin atomic charges are excellent; Pearson's R^2 ranges between 0.89 and 0.94 (also given in the insets of Figures 2A-2D). The Loewdin atomic charges are slightly better able to predict σ_p than σ_m , but are obviously excellent predictors of both quantities. For example, when using Loewdin atomic charges at carbon, the correlation with σ_p is $R^2 = 0.94$ and the correlation with σ_m is $R^2 = 0.90$. Similarly, when using Loewdin atomic charges at hydrogen, the correlation with σ_p is $R^2 = 0.93$ and the correlation with σ_m is $R^2 = 0.89$.

Unlike many previously examined charge models,⁹ where there is significant improvement when using hydrogen charges rather than carbon charges, the Loewdin atomic charge R^2 values remain about the same when using either carbon or hydrogen. This is true when considering the charges at either the meta and para positions. For ease of comparison, Table 1 presents the Pearson's R^2 values calculated here alongside some of the key previously published Pearson's R^2 values.⁹ Specifically, our new Loewdin results are compared to the published results for NPA, Hirshfeld, and CM5; the Hirshfeld and CM5 charge models were included because they provide strongly performing atomic charges that can be used as univariate predictor of σ_p and σ_m . NPA

was included because of its conceptual similarity to the Loewdin charge model; both are wave function-based projection schemes that improve upon Mulliken atomic charges with the use of orthogonalization. For the prediction of both σ_p and σ_m , Loewdin atomic charges show the strongest results, where the R^2 values all lie within the range of 0.89-0.94. This is somewhat in contrast to results from Hirshfeld and CM5 models, which exhibit a range of values from 0.84-0.91 and 0.83-0.91, respectively. In addition, the Loewdin atomic charges vastly outperform NPA charges despite the conceptual similarities between the methods, which exhibits a value of 0.12 for the σ_m vs $q(C_{\text{Meta}})$ correlation. The Loewdin approach, using its symmetrically orthogonalized atomic orbitals, is here seen to better handle the spatial proximity of the meta-substituents than the NPA approach, with its underlying natural atomic orbitals.

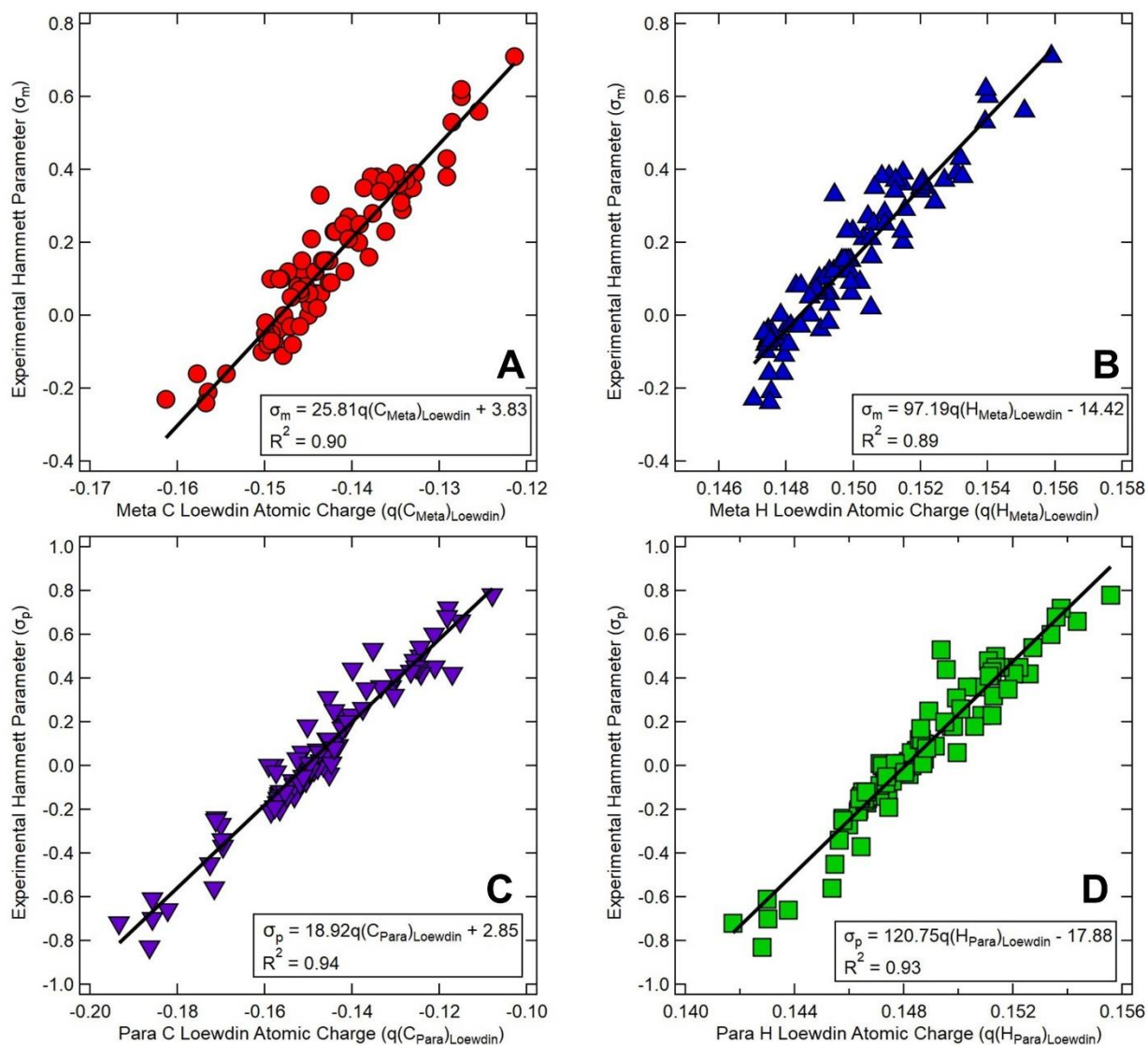


Figure 2. Experimental Hammett parameters correlated with **A** $q(C_{Meta})_{Loewdin}$ (red circles), **B** $q(H_{Meta})_{Loewdin}$ (blue triangles), **C** $q(C_{Para})_{Loewdin}$ (purple inverted triangles), or **D** $q(H_{Para})_{Loewdin}$ (green squares). The respective fit linear relationships are $\sigma_m = 25.81q(C_{Meta})_{Loewdin} + 3.83$, $\sigma_m = 97.19q(H_{Meta})_{Loewdin} - 14.42$, $\sigma_p = 18.92q(C_{Para})_{Loewdin} + 2.85$, and $\sigma_p = 120.75q(H_{Para})_{Loewdin} - 17.88$.

Table 1. Pearson's R^2 Values for Linear Correlations of Experimental Hammett Parameters with Computed Atomic Charges. The subscript 'X' corresponds to the given charge model.

	$X = \text{Loewdin}$	$X = \text{NPA}^a$	$X = \text{Hirshfeld}^a$	$X = \text{CM5}^a$
σ_m vs $q(\text{C}_{\text{Meta}})_X$	0.90	0.12	0.84	0.83
σ_p vs $q(\text{C}_{\text{Para}})_X$	0.94	0.86	0.92	0.92
σ_m vs $q(\text{H}_{\text{Meta}})_X$	0.89	0.86	0.87	0.87
σ_p vs $q(\text{H}_{\text{Para}})_X$	0.93	0.61	0.91	0.91

^aValues from Ref. 9.

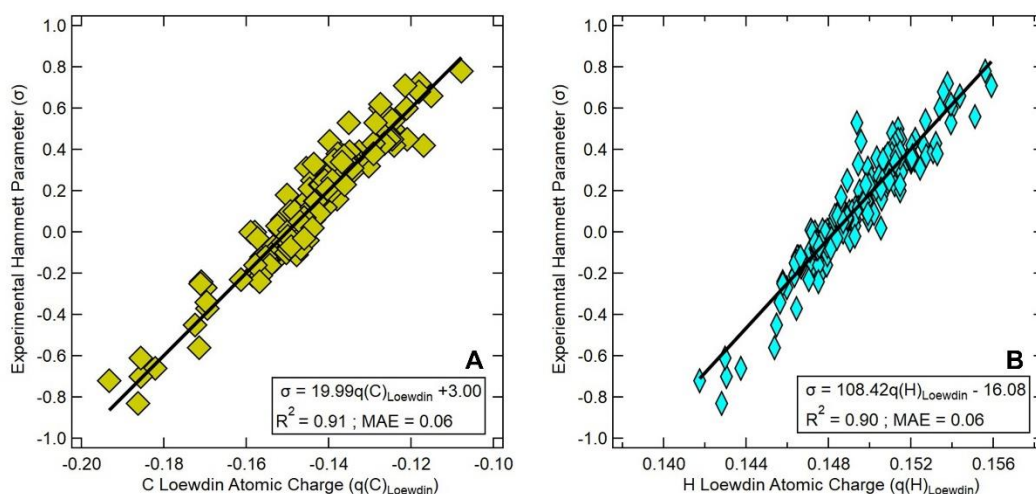


Figure 3. Concatenated experimental Hammett parameters correlated with **A** $q(\text{C})_{\text{Loewdin}}$ (gold diamonds), or **B** $q(\text{H})_{\text{Loewdin}}$ (cyan narrow diamonds). The respective linear fits are $\sigma = 19.99q(\text{C})_{\text{Loewdin}} + 3.00$ and $\sigma = 108.42q(\text{H})_{\text{Loewdin}} - 16.08$. When using either fit, the mean absolute error is calculated to be 0.06.

The quality of the correlation of the concatenated C and concatenated H atomic charge datasets (*i.e.*, simultaneous linear fitting where the meta and para datasets for a given atom type have been combined into a single dataset) was similarly assessed (Figure 3). MAE values were computed from the obtained linear relationships and the computed Loewdin atomic charges. Table 2 gives the Pearson's R^2 values for the newly calculated Loewdin datasets in comparison to

published results for NPA, Hirshfeld, and CM5. Table 3 has the MAEs from these same charge models of interest. The same overall trends are again observed as when prior to concatenation; Loewdin atomic charges on both carbons and hydrogens are seen to be excellent predictors of σ , and somewhat outperform Hirshfeld and CM5. The Loewdin errors (MAE = 0.06 when computed from either $q(\text{C})_{\text{Loewdin}}$ or $q(\text{H})_{\text{Loewdin}}$) are slightly lower than those previously obtained using Hirshfeld and CM5 (for both Hirshfeld and CM5 linear correlations, MAE = 0.07 when using either $q(\text{C})_{\text{Loewdin}}$ or $q(\text{H})_{\text{Loewdin}}$). In previous work, the Hirshfeld and CM5 were the best performing models judged by MAE when using either carbon or hydrogen atoms.⁹ When also considering R^2 , the Loewdin Pearson's R^2 values ($R^2 = 0.91$ using carbon, $R^2 = 0.90$ using hydrogen) are higher than both Hirshfeld ($R^2 = 0.87$ using carbon, $R^2 = 0.88$ using hydrogen) and CM5 results ($R^2 = 0.86$ using carbon, $R^2 = 0.88$ using hydrogen).

Table 2. Pearson's R^2 Values for Linear Correlations of Experimental Hammett Parameters with Computed Atomic Charges After Concatenation of Meta and Para Datasets. The subscript 'X' corresponds to the given charge model.

	$X = \text{Loewdin}$	$X = \text{NPA}^a$	$X = \text{Hirshfeld}^a$	$X = \text{CM5}^a$
σ vs $q(\text{C})_X$	0.91	0.45	0.87	0.86
σ vs $q(\text{H})_X$	0.90	0.59	0.88	0.88

^aValues from Ref. 9.

Table 3. Mean Absolute Error (MAE) Values from Linear Correlations of Experimental Hammett Parameters with Computed Atomic Charges After Concatenation of Meta and Para Datasets. The subscript 'X' corresponds to the given charge model.

	$X = \text{Loewdin}$	$X = \text{NPA}^a$	$X = \text{Hirshfeld}^a$	$X = \text{CM5}^a$
σ vs $q(\text{C})_X$	0.06	0.13	0.07	0.07
σ vs $q(\text{H})_X$	0.06	0.13	0.07	0.07

^aValues from Ref. 9.

Next, we have examined the linear correlation between experimental $\log_{10}(k_{\text{rel}})$ values for the cycloaddition of substituted nitroarenes with a model olefin substrate (admantylideneadamantane).^{9,19} Here $\log_{10}(k_{\text{rel}})$ is equivalent to $\log_{10}(k/k_{\text{H}})$ where k corresponds to the rate associated with the nitroarene of interest and k_{H} is the rate for nitrobenzene (the unsubstituted, reference nitroarene). The atomic charges on the carbon atom attached to the NO_2

group, $q(\text{C})_X$, and on the nitrogen atom within the NO_2 group, $q(\text{N})_X$ (' X ' corresponds to the charge model), were tabulated (these atomic positions are visually identified in Figure 1B). The quality of the correlation of these computed partial charges to experimental values of $\log_{10}(k_{\text{rel}})$ were assessed using linear fits and the resulting Pearson's R^2 value (Figures 4). As an additional new study, the atomic charges on both of the oxygen atoms within the NO_2 group in a given nitroarene were also tabulated. This allowed for assessment of the quality of the linear correlation to $\log_{10}(k_{\text{rel}})$ when using the averaged oxygen atomic charge, $q(\text{O}_{\text{Avg.}})_X$, or when using the total charge on the NO_2 group, $q(\text{NO}_2)_X$, (Figure 5). Figures 4 and 5 complement each other and together illuminate one situation where additive application of Loewdin charges is useful for prediction.

From Figure 4, one can see that all the linear correlations are extremely successful with the exception of the $\log_{10}(k_{\text{rel}})$ versus $q(\text{N})_{\text{Loewdin}}$ correlation (Figure 4B). For the other three correlations, the Pearson's R^2 values are excellent and range between 0.97 to 0.98. We note the similarities between the benchmark Hirshfeld results presented here and those previously published.⁹ Previously $R^2 = 0.94$ was observed when correlating $\log_{10}(k_{\text{rel}})$ to $q(\text{C})_{\text{Hirshfeld}}$ (here we newly calculate $R^2 = 0.98$); previously $R^2 = 0.94$ was observed when correlating $\log_{10}(k_{\text{rel}})$ to $q(\text{N})_{\text{Hirshfeld}}$ (here we newly calculate $R^2 = 0.97$). These modest differences could have arisen from differences between the quadrature grids used in the ORCA and Gaussian 16 calculations, the lack of a 3- NO_2 , 4-H, and 5- CF_3 structure in the present dataset (the 3- NO_2 , 4-H, and 5- CF_3 substituted nitroarene, appears not to have been uploaded to the database; instead, a non-experimental structure corresponding to 3- NO_2 , 4- CF_3 , and 5-H is available online)²⁶, and different choices regarding whether to average over multiple conformers or not.

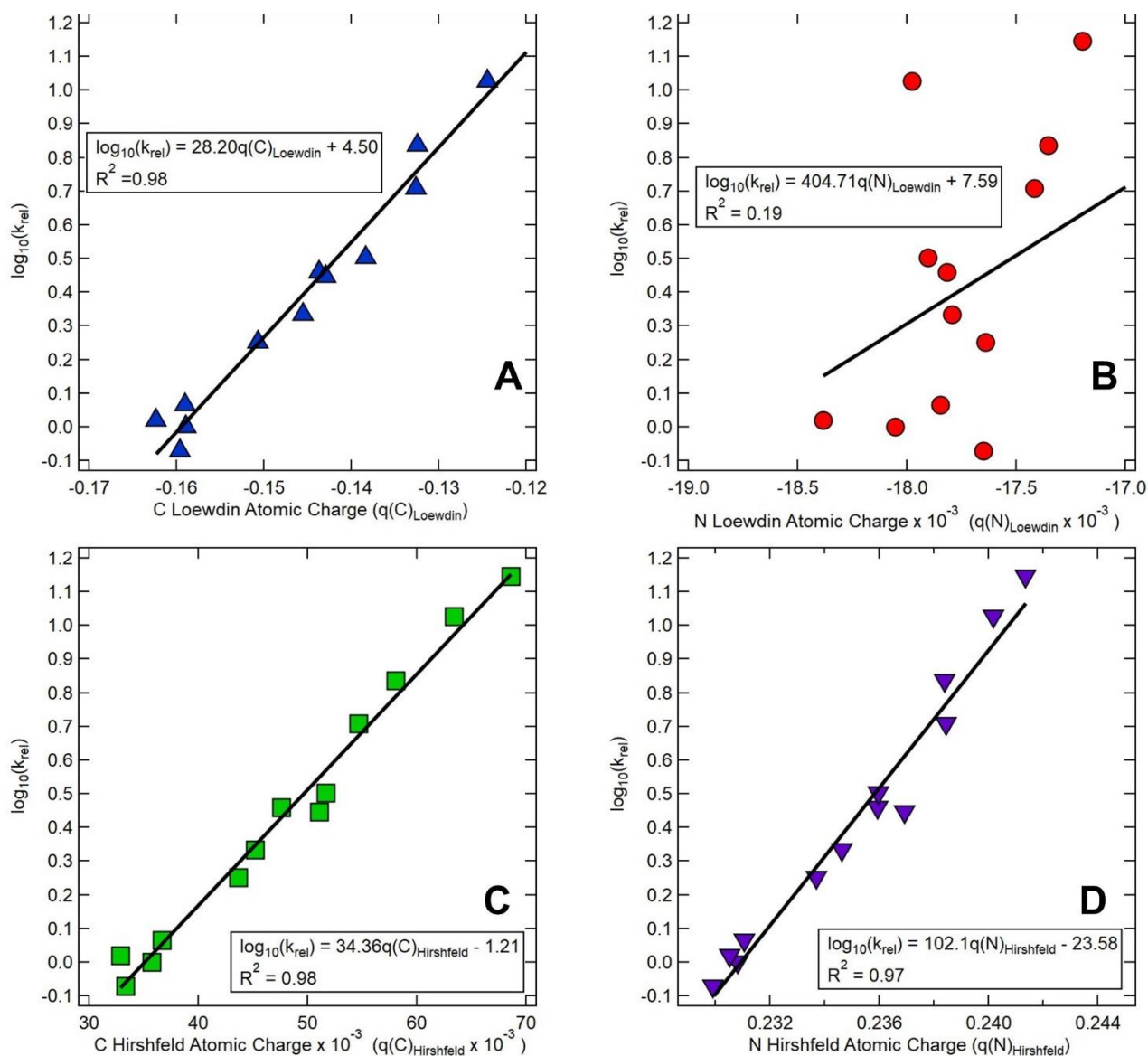


Figure 4. $\log_{10}(k_{\text{rel}})$ for olefin cleavage by photoexcited nitroarenes correlated with **A** $q(\text{C})_{\text{Loewdin}}$ (blue triangles), **B** $q(\text{N})_{\text{Loewdin}}$ (red circles), **C** $q(\text{C})_{\text{Hirshfeld}}$ (green squares), or **D** $q(\text{N})_{\text{Hirshfeld}}$ (purple inverted triangles). The respective linear fits are $\log_{10}(k_{\text{rel}}) = 28.20q(\text{C})_{\text{Loewdin}} + 4.50$, $\log_{10}(k_{\text{rel}}) = 404.71q(\text{N})_{\text{Loewdin}} + 7.59$, $\log_{10}(k_{\text{rel}}) = 34.36q(\text{C})_{\text{Hirshfeld}} - 1.21$, and $\log_{10}(k_{\text{rel}}) = 102.1q(\text{N})_{\text{Hirshfeld}} - 23.58$.

Table 4 has comparisons of Pearson's R^2 values obtained from key charge models of interest. While many of the charge models previously examined⁹ perform better when using $q(\text{N})_X$, Hirshfeld and CM5 perform very similarly regardless of whether $q(\text{N})_X$ or $q(\text{C})_X$ is used. Loewdin atomic charges, like NPA charges, perform significantly worse when using $q(\text{N})_X$. This is likely

related to similarities between the two methods and similar partitioning problems to which they both may be prone.

Table 4. Pearson's R^2 Values for Linear Correlations of Experimental Nitroarene Cycloaddition $\log_{10}(k_{rel})$ with Computed Atomic Charges on C and N. The subscript 'X' corresponds to the given charge model.

	$X = \text{Loewdin}^a$	$X = \text{NPA}^b$	$X =$ Hirshfeld ^a	$X =$ Hirshfeld ^b	$X = \text{CM5}^b$
$\log_{10}(k_{rel})$ vs $q(\text{C})_X$	0.98	0.42	0.98	0.94	0.94
$\log_{10}(k_{rel})$ vs $q(\text{N})_X$	0.19	0.00	0.97	0.94	0.94

^aThis work.

^bValues from Ref. 9.

It is possible to diagnose the origin of the failure to correlate $q(\text{N})_{\text{Loewdin}}$ with $\log_{10}(k_{rel})$ by considering the average charge on the two NO_2 oxygen atoms ($q(\text{O}_{\text{Avg.}})_X$, obtained from averaging the charges on O1 and O2 in Figure 1B) and the total overall charge on the NO_2 functional group ($q(\text{NO}_2)_X$, obtained from adding together the charges on N, O1, and O2 in Figure 1B). In Figure 5, one can see that all four correlations using $q(\text{O}_{\text{Avg.}})_X$ or $q(\text{NO}_2)_X$ are excellent. The general predictive, linear relationships from these fits are given in the figure, with Pearson's R^2 values of 0.97 from these four respective correlations. Tables S3 and S4 in the SI are useful to obtain a sense of the magnitudes of $q(\text{C})_X$, $q(\text{N})_X$, $q(\text{O}_{\text{Avg.}})_X$, and $q(\text{NO}_2)_X$. The values with by far the smallest magnitude are $q(\text{N})_{\text{Loewdin}}$. As a result, small inconsistencies in the Loewdin model's partitioning of charge between the NO_2 nitrogen and oxygen atoms cause there to be a poor $\log_{10}(k_{rel})$ versus $q(\text{N})_{\text{Loewdin}}$ correlation. Due to their larger overall magnitudes, the $q(\text{O}_{\text{Avg.}})_{\text{Loewdin}}$ values are less affected by these failures in partitioning. As a result, they are able provide a good, predictive linear correlation to $\log_{10}(k_{rel})$. The success of the correlation using $q(\text{NO}_2)_{\text{Loewdin}}$ shows that in cases of charge partitioning problems, the additive application of Loewdin charges (*i.e.*, using the total charge on a functional group rather than a single atomic charge) results in a useful predictive correlation.

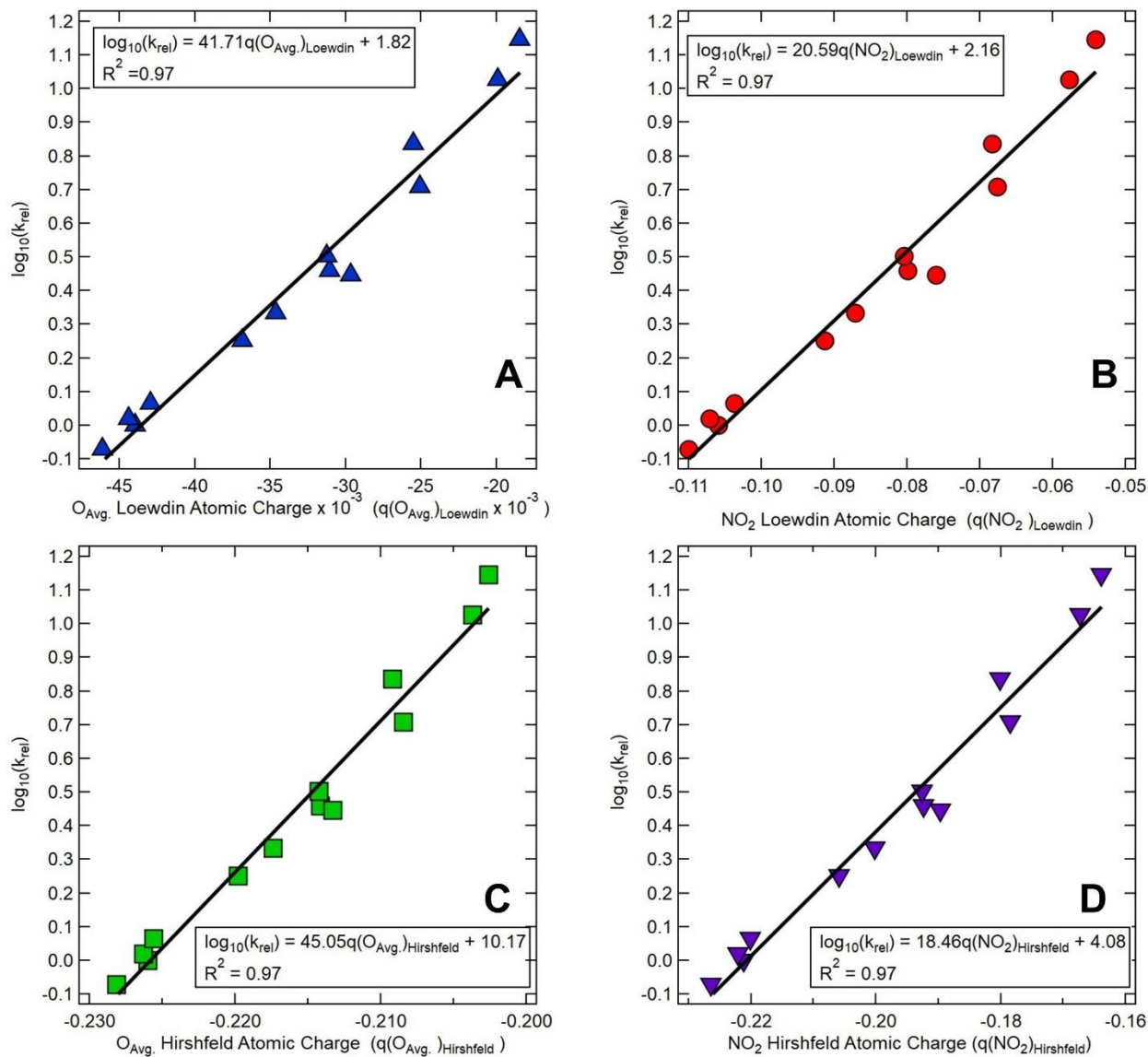


Figure 5. $\log_{10}(k_{rel})$ for olefin cleavage by photoexcited nitroarenes correlated with **A** $q(O_{Avg.})_{Loewdin}$ (blue triangles), **B** $q(NO_2)_{Loewdin}$ (red circles), **C** $q(O_{Avg.})_{Hirshfeld}$ (green squares), or **D** $q(NO_2)_{Hirshfeld}$ (purple inverted triangles). The respective linear fits are $\log_{10}(k_{rel}) = 41.71q(O_{Avg.})_{Loewdin} + 1.82$, $\log_{10}(k_{rel}) = 20.59q(NO_2)_{Loewdin} + 2.16$, $\log_{10}(k_{rel}) = 45.05q(O_{Avg.})_{Hirshfeld} + 10.17$, and $\log_{10}(k_{rel}) = 18.46q(NO_2)_{Hirshfeld} + 4.08$.

To further assess the quality of calculated atomic charges as univariate predictors of reaction rates, a series of 9-(4-X-phenyl)-9H-fluorene substrates were studied (X = OMe, CH₃, H, or CF₃). These substrates undergo C-H activation catalyzed by PhB(^tBuIm)₃Co^{III}O; the rates of these activations have been shown to correlate with experimentally known σ_p^- parameters despite

the inherently complex chemistry.^{24,25} The large, extended nature of these substrates make them attractive test case for the application of univariate, correlative methodologies. For example, in Figure 1C one sees that there are many atomic charges that could potentially be correlated to observed rates. Here we have used atomic charges on the atoms identified as C1, C2, and H1. Loewdin, Hirshfeld, and CM5 atomic charges were tabulated for C1, C2, and the H1 atoms identified on the generalized substrate in Figure 1C (charge values from all calculations are tabulated in the SI).

The complexity of these chemical systems and their underlying proton transfer mechanisms bear further description. It has been demonstrated these C-H activations often involve a single, asynchronous concerted proton electron transfer (CPET) step, but can mechanistically crossover to stepwise reactivity depending on substrate identity.⁴³ Through variable temperature kinetic isotope effects, it has been shown that these processes can involve quantum mechanical tunneling of the transferred proton.⁴⁴ It has theoretically been shown that the rate of the nonadiabatic CPET step should logically increase with a decrease in the stepwise thermodynamic parameter of only proton transfer (ΔG_{PT}).⁴⁵ As explained by Schneider and Anderson, this results from increased anharmonicity of the reactant state (and, in turn, increased proton tunneling) due to a large electronic coupling between the reactant state and the proton-only transfer state. Interestingly, the systematic tuning of potential energy surfaces, although not for a system involving proton tunneling, has also been described for the entatic photochemistry of copper(I) bis-phenanthrolines.⁴⁶ Given the complexity and richness of the 9-(4-X-phenyl)-9H-fluorene C-H activation chemistry, these substrates constitute a rigorous test case for the univariate, predictive approach. Furthermore, like the nitroarene molecules, these large substituted substrate molecules allow one to examine atomic charges on atoms more than one atom away from the aromatic ring.

Figure 6 shows linear correlations between the experimental $\log_{10}(k_{rel})$ for C-H activation (referenced to the X = H rate, Figure 1C) and the computed atomic charge values of $q(C1)_X$, $q(C2)_X$, and $q(H1)_X$; specifically, the data obtained from using B3LYP and the $S = 0$ spin multiplicity are shown. While all the computed correlations are strong, the Hirshfeld correlations using C2 (Figure 6E; $R^2 = 0.989$) and H1 (Figure 6F; $R^2 = 0.995$) are particularly excellent, though the Loewdin correlation using C2 (Figure 6B; $R^2 = 0.976$) is comparable. For comparison, the correlation to the experimental σ_p^- parameters has been noted by Goetz and Anderson to be 0.996.^{24,25} The

respective general, predictive linear relationships are given in the Figure 6 insets. Similar results are seen when considering B3LYP and the $S = 1$ spin multiplicity (Figure S2).

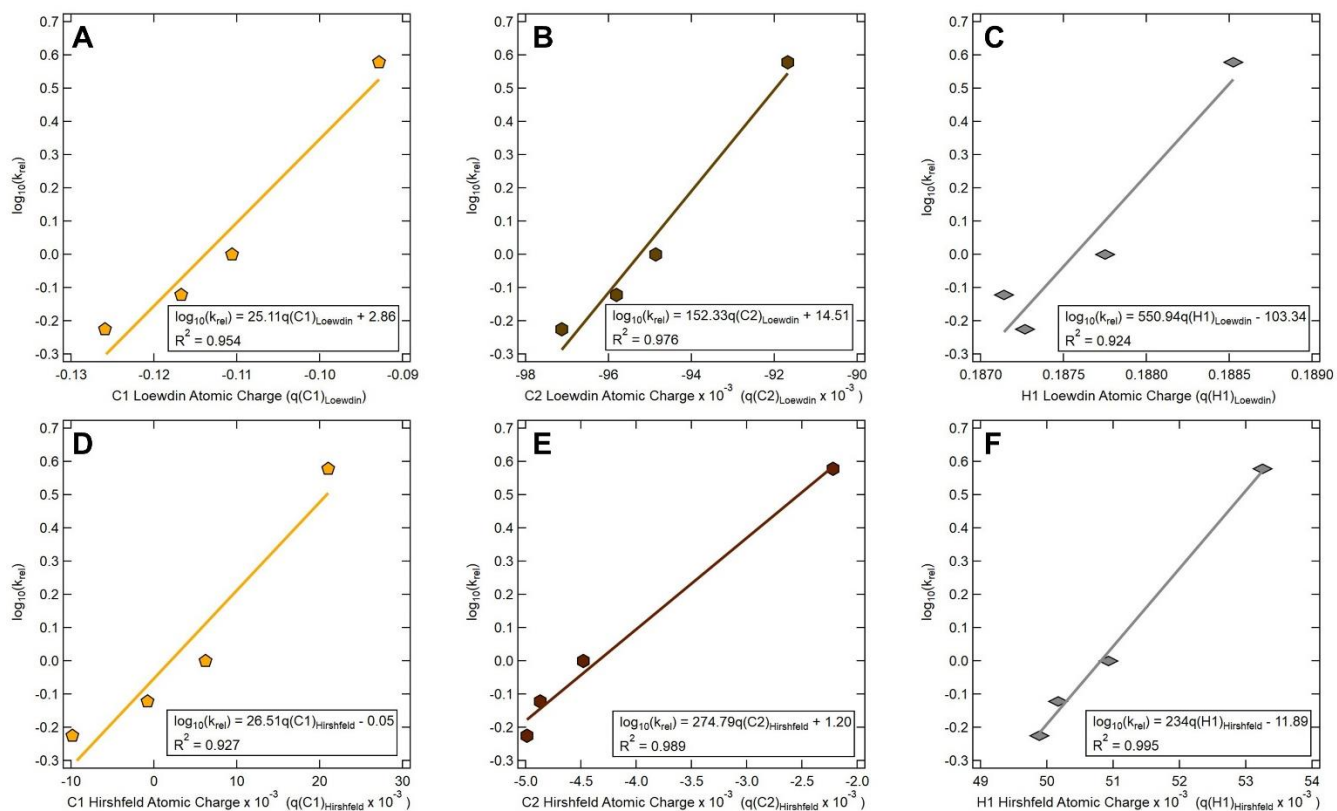


Figure 6. $\log_{10}(k_{rel})$ for C-H activation of 9-(4-X-phenyl)-9H-fluorenes (X = OMe, CH₃, H, or CF₃) by PhB(^tBuIm)₃Co^{III}O correlated with **A** $q(C1)_{Loewdin}$ (yellow pentagons), **B** $q(C2)_{Loewdin}$ (brown hexagons), **C** $q(H1)_{Loewdin}$ (gray wide diamonds), **D** $q(C1)_{Hirshfeld}$ (yellow pentagons), **E** $q(C2)_{Hirshfeld}$ (brown hexagons), or **F** $q(H1)_{Hirshfeld}$ (gray wide diamonds). The atomic charges presented here came from the $S = 0$ B3LYP single point calculations described in the Computational Methods. The respective linear fits are $\log_{10}(k_{rel}) = 25.11q(C1)_{Loewdin} + 2.86$, $\log_{10}(k_{rel}) = 152.33q(C2)_{Loewdin} + 14.51$, $\log_{10}(k_{rel}) = 550.94q(H1)_{Loewdin} - 103.34$, $\log_{10}(k_{rel}) = 26.51q(C1)_{Hirshfeld} - 0.05$, $\log_{10}(k_{rel}) = 274.79q(C2)_{Hirshfeld} + 1.20$, and $\log_{10}(k_{rel}) = 234q(H1)_{Hirshfeld} - 11.89$.

A complete list of Pearson's R^2 values from different linear correlations for the $S = 0$ spin multiplicity are shown in Table 5. These include Hirshfeld charges for 9-(4-X-phenyl)-9H-fluorenes computed with the M06-L functional (Figure S3), and CM5 charges also computed with

M06-L (Figure S4). The M06-L functional was used in this case to provide an initial test of the exchange-correlation functional on the computed linear correlations. In Table 5 one sees that for both Hirshfeld datasets and the CM5 dataset, there is a notable improvement in the R^2 value when using charges from C2 or H1 rather than from C1. This is another instance where the use of atoms further from the aromatic ring improves the linear correlation for Hirshfeld and CM5. In contrast, this is somewhat reversed in the Loewdin atomic results, where C2 gives the best correlations, followed by C1, and then followed by H1. Again, similar results are seen when considering the $S = 1$ spin multiplicity (Figures S2-S4). We also observe that all charge models tested here yield similar overall accuracy, with relatively small changes in R^2 value due to choice of functional.

Table 5. Pearson's R^2 Values for Linear Correlations of 9-(4-X-phenyl)-9H-fluorene ($S = 0$) C-H activation $\log_{10}(k_{\text{rel}})$ with Computed Atomic Charges on C1, C2, and H1. The subscript 'X' corresponds to the given charge model.

	$X = \text{Loewdin}^a$	$X = \text{Hirshfeld}^a$	$X = \text{Hirshfeld}^b$	$X = \text{CM5}^b$
$\log_{10}(k_{\text{rel}})$ vs $q(\text{C1})_X (S = 0)$	0.954	0.927	0.900	0.902
$\log_{10}(k_{\text{rel}})$ vs $q(\text{C2})_X (S = 0)$	0.976	0.989	0.996	0.995
$\log_{10}(k_{\text{rel}})$ vs $q(\text{H1})_X (S = 0)$	0.924	0.995	0.996	0.994

^aB3LYP single point calculations described in the Computational Methods section.

^bM06-L geometry optimizations described in the Computational Methods section.

Conclusions

It has been shown here that Loewdin atomic charges can be very successfully used as univariate, linear predictors of σ_p values, of σ_m values, and of select $\log_{10}(k_{\text{rel}})$ values. Indeed, using Loewdin atomic charges yields lower errors in σ compared to when using Hirshfeld and CM5 charges. In addition, Loewdin atomic charges are often consistently strong univariate predictors whether obtained from the aromatic ring of interest or from an attached, more distant atom. We also show that Loewdin charges are useful predictors of $\log_{10}(k_{\text{rel}})$ values for both olefin cleavage by photoexcited nitroarenes and C-H activation of 9-(4-X-phenyl)-9H-fluorene

substrates by a transition metal catalyst. Our nitroarene study highlights the utility of predictive correlations based on the additive application of Loewdin atomic charges, where determination of correlations with the net NO₂ charge rather than the nitrogen charge alone yielded a strong predictive capability. Our C-H activation results demonstrate that univariate linear, predictive methodologies based on computed atomic charges can be established for very chemically complex processes involving large substrates. Given the observed agreement between charge model results in periodic materials and results from related molecular cluster models,⁴⁷ we note that atomic charges likely have the potential to be successful univariate linear predictors of log₁₀(k_{rel}) in extended materials, which is the subject of future work. The linear, correlative equations obtained here are useful to investigations attempting to computationally predict σ_p , σ_m , and relative reaction rates, where rapid screening of chemical reactivity can aid the design of compounds and materials with tailored properties.

ASSOCIATED CONTENT

Supporting Information. Example ORCA 5.0.4 and Gaussian 16 input files, tabulations of computed energies and atomic charges, and additional plotted linear correlations discussed in this manuscript are provided in the Supplement Information PDF file. The Loewdin atomic charges for the 89 substituted benzene molecules are provided as six uploaded text files.

The following files are available free of charge.

Supplement-Information.pdf (PDF)
LOEWDIN-META-C1.txt (text file)
LOEWDIN-PARA-C2.txt (text file)
LOEWDIN-META-C3.txt (text file)
LOEWDIN-META-H1.txt (text file)
LOEWDIN-PARA-H2.txt (text file)
LOEWDIN-META-H3.txt (text file)

AUTHOR INFORMATION

Corresponding Author

*Email Addresses: strosiol@llnl.gov ; gstroschio@uchicago.edu

Author Contributions

G. D. S. conceived the study, performed the electronic structure calculations, and wrote the manuscript. N. G. contributed to the writing and editing of the manuscript. All authors have given approval to the final version of the manuscript.

ACKNOWLEDGMENT

This work was performed under the auspices of the U.S. Department of Energy by Lawrence Livermore National Laboratory under Contract DE-AC52-07NA27344.

REFERENCES

- (1) Hammett, L. P. Some Relations between Reaction Rates and Equilibrium Constants. *Chem. Rev.* **1935**, *17* (1), 125–136. <https://doi.org/10.1021/cr60056a010>.
- (2) Hammett, L. P. The Effect of Structure upon the Reactions of Organic Compounds. Benzene Derivatives. *J. Am. Chem. Soc.* **1937**, *59* (1), 96–103. <https://doi.org/10.1021/ja01280a022>.
- (3) Hansch, Corwin.; Leo, A.; Taft, R. W. A Survey of Hammett Substituent Constants and Resonance and Field Parameters. *Chem. Rev.* **1991**, *91* (2), 165–195. <https://doi.org/10.1021/cr00002a004>.
- (4) Williams, W. L.; Zeng, L.; Gensch, T.; Sigman, M. S.; Doyle, A. G.; Anslyn, E. V. The Evolution of Data-Driven Modeling in Organic Chemistry. *ACS Cent. Sci.* **2021**, *7* (10), 1622–1637. <https://doi.org/10.1021/acscentsci.1c00535>.
- (5) Brown, H. C.; Okamoto, Y. Electrophilic Substituent Constants. *J. Am. Chem. Soc.* **1958**, *80* (18), 4979–4987. <https://doi.org/10.1021/ja01551a055>.
- (6) Creary, X.; Mehrsheikh-Mohammadi, M. E.; McDonald, S. Methylene-cyclopropane Rearrangement as a Probe for Free Radical Substituent Effects. *Sigma.Bul. Values for Commonly Encountered Conjugating and Organometallic Groups. J. Org. Chem.* **1987**, *52* (15), 3254–3263. <https://doi.org/10.1021/jo00391a015>.
- (7) Jiang, X.; Ji, G. A Self-Consistent and Cross-Checked Scale of Spin-Delocalization Substituent Constants, the *Sigma.JJ.Bul. Scale. J. Org. Chem.* **1992**, *57* (22), 6051–6056. <https://doi.org/10.1021/jo00048a048>.
- (8) Dust, J. M.; Arnold, D. R. Substituent Effects on Benzyl Radical ESR Hyperfine Coupling Constants. The *Sigma.Alpha.Cntdot. Scale Based upon Spin Delocalization. J. Am. Chem. Soc.* **1983**, *105* (5), 1221–1227. <https://doi.org/10.1021/ja00343a024>.
- (9) Luchini, G.; Paton, R. S. Bottom-Up Atomistic Descriptions of Top-Down Macroscopic Measurements: Computational Benchmarks for Hammett Electronic Parameters. *ACS Phys. Chem. Au* **2024**, *4* (3), 259–267. <https://doi.org/10.1021/acsphyschemau.3c00045>.

- (10) Monteiro-de-Castro, G.; Duarte, J. C.; Borges, I. Jr. Machine Learning Determination of New Hammett's Constants for Meta- and Para-Substituted Benzoic Acid Derivatives Employing Quantum Chemical Atomic Charge Methods. *J. Org. Chem.* **2023**, *88* (14), 9791–9802. <https://doi.org/10.1021/acs.joc.3c00410>.
- (11) Ertl, P. A Web Tool for Calculating Substituent Descriptors Compatible with Hammett Sigma Constants. *Chemistry–Methods* **2022**, *2* (12), e202200041. <https://doi.org/10.1002/cmt.202200041>.
- (12) Storer, J. W.; Giesen, D. J.; Cramer, C. J.; Truhlar, D. G. Class IV Charge Models: A New Semiempirical Approach in Quantum Chemistry. *J. Comput. Aided Mol. Des.* **1995**, *9* (1), 87–110. <https://doi.org/10.1007/BF00117280>.
- (13) Cho, M.; Sylvetsky, N.; Eshafi, S.; Santra, G.; Efremenko, I.; Martin, J. M. L. The Atomic Partial Charges Arboretum: Trying to See the Forest for the Trees. *ChemPhysChem* **2020**, *21* (8), 688–696. <https://doi.org/10.1002/cphc.202000040>.
- (14) Mulliken, R. S. Electronic Population Analysis on LCAO–MO Molecular Wave Functions. I. *J. Chem. Phys.* **1955**, *23* (10), 1833–1840. <https://doi.org/10.1063/1.1740588>.
- (15) Reed, A. E.; Weinstock, R. B.; Weinhold, F. Natural Population Analysis. *J. Chem. Phys.* **1985**, *83* (2), 735–746. <https://doi.org/10.1063/1.449486>.
- (16) Reed, A. E.; Curtiss, L. A.; Weinhold, F. Intermolecular Interactions from a Natural Bond Orbital, Donor-Acceptor Viewpoint. *Chem. Rev.* **1988**, *88* (6), 899–926. <https://doi.org/10.1021/cr00088a005>.
- (17) Hirshfeld, F. L. Bonded-Atom Fragments for Describing Molecular Charge Densities. *Theor. Chim. Acta* **1977**, *44* (2), 129–138. <https://doi.org/10.1007/BF00549096>.
- (18) Marenich, A. V.; Jerome, S. V.; Cramer, C. J.; Truhlar, D. G. Charge Model 5: An Extension of Hirshfeld Population Analysis for the Accurate Description of Molecular Interactions in Gaseous and Condensed Phases. *J. Chem. Theory Comput.* **2012**, *8* (2), 527–541. <https://doi.org/10.1021/ct200866d>.
- (19) Ruffoni, A.; Hampton, C.; Simonetti, M.; Leonori, D. Photoexcited Nitroarenes for the Oxidative Cleavage of Alkenes. *Nature* **2022**, *610* (7930), 81–86. <https://doi.org/10.1038/s41586-022-05211-0>.
- (20) Löwdin, P. On the Non-Orthogonality Problem Connected with the Use of Atomic Wave Functions in the Theory of Molecules and Crystals. *J. Chem. Phys.* **1950**, *18* (3), 365–375. <https://doi.org/10.1063/1.1747632>.
- (21) Löwdin, P. Approximate Formulas for Many-Center Integrals in the Theory of Molecules and Crystals. *J. Chem. Phys.* **1953**, *21* (2), 374–375. <https://doi.org/10.1063/1.1698901>.
- (22) Sauza-de la Vega, A.; Pandharkar, R.; Strocio, G. D.; Sarkar, A.; Truhlar, D. G.; Gagliardi, L. Multiconfiguration Pair-Density Functional Theory for Chromium(IV) Molecular Qubits. *JACS Au* **2022**, *2* (9), 2029–2037. <https://doi.org/10.1021/jacsau.2c00306>.
- (23) Strocio, G. D.; Srnc, M.; Hadt, R. G. Multireference Ground and Excited State Electronic Structures of Free- versus Iron Porphyrin-Carbenes. *Inorg. Chem.* **2020**, *59* (13), 8707–8715. <https://doi.org/10.1021/acs.inorgchem.0c00249>.
- (24) Goetz, M. K.; Anderson, J. S. Experimental Evidence for pKa-Driven Asynchronicity in C–H Activation by a Terminal Co(III)–Oxo Complex. *J. Am. Chem. Soc.* **2019**, *141* (9), 4051–4062. <https://doi.org/10.1021/jacs.8b13490>.
- (25) Goetz, M. K.; Anderson, J. S. Correction to “Experimental Evidence for pKa-Driven Asynchronicity in C–H Activation by a Terminal Co(III)–Oxo Complex.” *J. Am. Chem. Soc.* **2020**, *142* (11), 5439–5441. <https://doi.org/10.1021/jacs.0c02031>.

- (26) <https://github.com/patonlab/SI-Hammett-Computational-Data> (Accessed 6-10-2024).
- (27) Becke, A. D. Density-Functional Exchange-Energy Approximation with Correct Asymptotic Behavior. *Phys. Rev. A* **1988**, *38* (6), 3098–3100. <https://doi.org/10.1103/PhysRevA.38.3098>.
- (28) Lee, C.; Yang, W.; Parr, R. G. Development of the Colle-Salvetti Correlation-Energy Formula into a Functional of the Electron Density. *Phys. Rev. B* **1988**, *37* (2), 785–789. <https://doi.org/10.1103/PhysRevB.37.785>.
- (29) Weigend, F.; Ahlrichs, R. Balanced Basis Sets of Split Valence, Triple Zeta Valence and Quadruple Zeta Valence Quality for H to Rn: Design and Assessment of Accuracy. *Phys. Chem. Chem. Phys.* **2005**, *7* (18), 3297–3305. <https://doi.org/10.1039/B508541A>.
- (30) Weigend, F. Accurate Coulomb-Fitting Basis Sets for H to Rn. *Phys. Chem. Chem. Phys.* **2006**, *8* (9), 1057–1065. <https://doi.org/10.1039/B515623H>.
- (31) Grimme, S.; Antony, J.; Ehrlich, S.; Krieg, H. A Consistent and Accurate Ab Initio Parametrization of Density Functional Dispersion Correction (DFT-D) for the 94 Elements H–Pu. *J. Chem. Phys.* **2010**, *132* (15), 154104. <https://doi.org/10.1063/1.3382344>.
- (32) Grimme, S.; Ehrlich, S.; Goerigk, L. Effect of the Damping Function in Dispersion Corrected Density Functional Theory. *J. Comput. Chem.* **2011**, *32* (7), 1456–1465. <https://doi.org/10.1002/jcc.21759>.
- (33) Marenich, A. V.; Cramer, C. J.; Truhlar, D. G. Universal Solvation Model Based on Solute Electron Density and on a Continuum Model of the Solvent Defined by the Bulk Dielectric Constant and Atomic Surface Tensions. *J. Phys. Chem. B* **2009**, *113* (18), 6378–6396. <https://doi.org/10.1021/jp810292n>.
- (34) Neese, F. The ORCA Program System. *WIREs Comput. Mol. Sci.* **2012**, *2* (1), 73–78. <https://doi.org/10.1002/wcms.81>.
- (35) Neese, F. Software Update: The ORCA Program System, Version 4.0. *WIREs Comput. Mol. Sci.* **2018**, *8* (1), e1327. <https://doi.org/10.1002/wcms.1327>.
- (36) Neese, F.; Wennmohs, F.; Becker, U.; Riplinger, C. The ORCA Quantum Chemistry Program Package. *J. Chem. Phys.* **2020**, *152* (22), 224108. <https://doi.org/10.1063/5.0004608>.
- (37) Neese, F. Software Update: The ORCA Program System—Version 5.0. *WIREs Comput. Mol. Sci.* **2022**, *12* (5), e1606. <https://doi.org/10.1002/wcms.1606>.
- (38) Neese, F. The SHARK Integral Generation and Digestion System. *J. Comput. Chem.* **2023**, *44* (3), 381–396. <https://doi.org/10.1002/jcc.26942>.
- (39) Neese, F.; Wennmohs, F.; Hansen, A.; Becker, U. Efficient, Approximate and Parallel Hartree–Fock and Hybrid DFT Calculations. A ‘Chain-of-Spheres’ Algorithm for the Hartree–Fock Exchange. *Mov. Front. Quantum Chem.* **2009**, *356* (1), 98–109. <https://doi.org/10.1016/j.chemphys.2008.10.036>.
- (40) Peterson, K. A.; Figgen, D.; Goll, E.; Stoll, H.; Dolg, M. Systematically Convergent Basis Sets with Relativistic Pseudopotentials. II. Small-Core Pseudopotentials and Correlation Consistent Basis Sets for the Post-d Group 16–18 Elements. *J. Chem. Phys.* **2003**, *119* (21), 11113–11123. <https://doi.org/10.1063/1.1622924>.
- (41) Zhao, Y.; Truhlar, D. G. A New Local Density Functional for Main-Group Thermochemistry, Transition Metal Bonding, Thermochemical Kinetics, and Noncovalent Interactions. *J. Chem. Phys.* **2006**, *125* (19), 194101. <https://doi.org/10.1063/1.2370993>.
- (42) Frisch, M. J.; Trucks, G. W.; Schlegel, H. B.; Scuseria, G. E.; Robb, M. A.; Cheeseman, J. R.; Scalmani, G.; Barone, V.; Petersson, G. A.; Nakatsuji, H.; Li, X.; Caricato, M.; Marenich, A. V.; Bloino, J.; Janesko, B. G.; Gomperts, R.; Mennucci, B.; Hratchian, H. P.; Ortiz, J. V.;

- Izmaylov, A. F.; Sonnenberg, J. L.; Williams-Young, D.; Ding, F.; Lipparini, F.; Egidi, F.; Goings, J.; Peng, B.; Petrone, A.; Henderson, T.; Ranasinghe, D.; Zakrzewski, V. G.; Gao, J.; Rega, N.; Zheng, G.; Liang, W.; Hada, M.; Ehara, M.; Toyota, K.; Fukuda, R.; Hasegawa, J.; Ishida, M.; Nakajima, T.; Honda, Y.; Kitao, O.; Nakai, H.; Vreven, T.; Throssell, K.; Montgomery, J. A., Jr.; Peralta, J. E.; Ogliaro, F.; Bearpark, M. J.; Heyd, J. J.; Brothers, E. N.; Kudin, K. N.; Staroverov, V. N.; Keith, T. A.; Kobayashi, R.; Normand, J.; Raghavachari, K.; Rendell, A. P.; Burant, J. C.; Iyengar, S. S.; Tomasi, J.; Cossi, M.; Millam, J. M.; Klene, M.; Adamo, C.; Cammi, R.; Ochterski, J. W.; Martin, R. L.; Morokuma, K.; Farkas, O.; Foresman, J. B.; Fox, D. J. Gaussian 16 Revision A.03; Gaussian Inc.: Wallingford, CT, **2016**.
- (43) Zhao, N.; Goetz, M. K.; Schneider, J. E.; Anderson, J. S. Testing the Limits of Imbalanced CPET Reactivity: Mechanistic Crossover in H-Atom Abstraction by Co(III)–Oxo Complexes. *J. Am. Chem. Soc.* **2023**, *145* (10), 5664–5673. <https://doi.org/10.1021/jacs.2c10553>.
- (44) Schneider, J. E.; Goetz, M. K.; Anderson, J. S. Variable Temperature Kinetic Isotope Effects Demonstrate Extensive Tunnelling in the C–H Activation Reactivity of a Transition Metal-Oxo Complex. *Chem. Commun.* **2023**, *59* (55), 8584–8587. <https://doi.org/10.1039/D3CC02130K>.
- (45) Schneider, J. E.; Anderson, J. S. Reconciling Imbalanced and Nonadiabatic Reactivity in Transition Metal–Oxo-Mediated Concerted Proton Electron Transfer (CPET). *J. Phys. Chem. Lett.* **2023**, *14* (43), 9548–9555. <https://doi.org/10.1021/acs.jpcclett.3c02318>.
- (46) Strocio, G. D.; Ribson, R. D.; Hadt, R. G. Quantifying Entatic States in Photophysical Processes: Applications to Copper Photosensitizers. *Inorg. Chem.* **2019**, *58* (24), 16800–16817. <https://doi.org/10.1021/acs.inorgchem.9b02976>.
- (47) Shohel, M.; Bustos, J.; Strocio, G. D.; Sarkar, A.; Nyman, M. Elucidating Actinide–Pertechnetate and Actinide–Perrhenate Bonding via a Family of Th–TcO₄ and Th–ReO₄ Frameworks and Solutions. *Inorg. Chem.* **2023**, *62* (26), 10450–10460. <https://doi.org/10.1021/acs.inorgchem.3c01430>.

For Table of Contents Only

